Stacking-dependent magnetoelectronic properties in multilayer graphene

Chiun-Yan Lin,[1] Jhao-Ying Wu,[2] Yu-Huang Chiu,[2,*] Cheng-Pong Chang,[3,†] and Ming-Fa Lin[1,‡]
[1]*Department of Physics, National Cheng Kung University, Tainan, Taiwan*
[2]*National Center for Theoretical Science, Taiwan*
[3]*Center for General Education, Tainan University of Technology, Tainan, Taiwan*
(Received 30 July 2014; revised manuscript received 9 November 2014; published 25 November 2014)

The generalized Peierls tight-binding model is developed to study multilayer graphenes. For an N-layer system, there are N groups of conduction and valence Landau levels. Each group is clearly specified by the corresponding sublattice. The Landau-level spectra strongly depend on the stacking configuration. ABC-stacked graphenes exhibit two kinds of Landau-level anticrossings, the intergroup and intragroup Landau levels, as a function of the applied magnetic field. On the other hand, in contrast to its frequent wide-energy presence in ABC-stacked graphenes, the anticrossing only occurs occasionally in AB-stacked graphenes, and is absent in AA-stacked graphenes. Furthermore, all $4N$ Dirac-point related Landau levels are distributed over a limited energy range near the Fermi level. In AA- and AB-stacked graphenes, the total number of such levels is fixed, while their energies depend on the stacking configuration. These results reflect the main features of the zero-field band structures.

DOI: 10.1103/PhysRevB.90.205434 PACS number(s): 81.05.U−, 78.67.Pt, 71.70.Di

I. INTRODUCTION

Ever since few-layer graphenes were first fabricated from highly oriented pyrolytic graphite via exfoliation procedures [1,2], they have attracted considerable experimental and theoretical interest. Being held together by van der Waals interactions, the graphene sheets are essentially stacked in AA [3], AB [4–10], or ABC [7–11] sequence along the perpendicular direction, with the respective geometric structures contributing to very distinct electronic properties [12–22]. The unique electronic structures have been experimentally verified by angle-resolved photoemission spectroscopy [23–25]. In particular, the main features of magnetoelectronic properties are associated with the zero-field band structure [26–32], including the energy spectrum, classification, and anticrossing of Landau levels (LLs). Subsequently, further investigation brought to light other intriguing physical properties, e.g., the Coulomb excitations [33,34], optical properties [26,35], and the quantum Hall transport properties [36–41].

Layered graphene is a gapless 2D semimetal with a slight overlap between valence bands and conduction bands [14,16,18], whereas a tunable energy gap is introduced in AB bilayer [42–46], and ABC trilayer graphenes [47–49] subjected to an external electric field. In the presence of a uniform perpendicular magnetic field ($\mathbf{B} = \mathbf{B_0}\hat{\mathbf{z}}$), the energy bands evolve into dispersionless LLs. The important anticrossing phenomenon among the LLs has been investigated in biased few-layer AB-stacked graphene [50–55] and in the bulk graphite [56]. Another crucial issue is the splitting of the zero-energy LLs that result from the Dirac-point properties [36,40]. While recent experimental observations on the quantum Hall effects (QHE) reveal the LL crossing, the plateau shift and the specific sequence of plateaus of QHE conductivity in trilayer graphene [40,41,55], studying other layer systems is worthwhile in terms of determining the dependence of the unique LL properties on the layer number and the stacking sequence.

In the absence of an external field, the low-energy electronic structure of ABC-stacked graphene consists of one pair of weakly dispersive bands at the Fermi level ($E_F = 0$) and a few other bands crossing at K point, which constitute a hybridization of hyperbolic, linear and mexican-hat bands [16,18,25]. In contrast, AA- and AB-stacked graphenes possess relatively simple band structures which resemble monolayer or bilayer graphene, or a hybridization of both [12,13,15]. Previous works have shown that in AA-stacked systems, the LL spectrum exhibits the monolayerlike energy dependence [26], while in AB-stacked systems, the characteristic of the monolayer spectrum is presented in the cases of odd number of stacking layers [29]. In this work, we show that the peculiarity of the band structure in ABC-stacked graphenes leads to the LL evolution under a magnetic field revealing a complex pattern of LL anticrossings, especially in the region of weak fields, as a result of the specific interlayer atomic interactions from the full tight-binding model. With an increasing number of layers, the magnetoelectronic properties are enriched and diversified. It should be noted that the few Dirac-point related LLs are confined in a small energy range around $E_F = 0$. The total number of such LLs is fixed for AA- and AB-stacked graphenes, while their energies are dependent on the stacking configurations.

In the generalized tight-binding model, the sublattice dominance is evidently derived from the Landau wave functions. Due to the relationship between the Landau state and the sublattice dominance, LLs can be classified without ambiguity, and quantum numbers are straightforwardly defined. Interlayer atomic interactions lead to versatile electronic properties, to an extent that even remote interactions are important. The Landau wave functions consisting of multizero modes can explain the anticrossings of LLs in terms of the perturbation theory. The obtained results are useful for further research on the essential physical properties. In Sec. II, the Hamiltonian is built from the Peierls tight-binding model in **B**. A discussion

*airegg.py90g@nctu.edu.tw
†t00252@mail.tut.edu.tw
‡mflin@mail.ncku.edu.tw

on the LL energy spectrum and the Landau wave functions is offered in Sec. III, where the sublattice dominance is identified and utilized to define each LL quantum number. Other spectrum features are investigated as well, including the sublattice dominance, the field-dependent energies and the inter- and intragroup anticrossings. Meanwhile, the aforementioned results are compared to AA- and AB-stacked graphenes. Investigation of the anticrossing patterns amongst these systems is a worthwhile undertaking. Finally, Sec. IV contains concluding remarks.

II. THE PEIERLS TIGHT-BINDING MODEL

ABC-stacked graphene has an interlayer distance of $d = 3.37$ Å and a bond length of $b' = 1.42$ Å, as sketched in Fig. 1(a). For an N-layer system, there are $2N$ carbon atoms per primitive unit cell where two sublattice atoms in the nth layer are denoted as A^n and B^n. Each of the graphene sheets is shifted by a distance of b' along the armchair direction with respect to the adjacent layer. The sublattice B (black dots) of one layer is situated directly above the A atom of the adjacent lower layer, whereas sublattice A (red dots) lies above the center of its hexagon. The low-energy electronic properties, mainly arising from the $2p_z$ orbitals, are described by the tight-binding model. The Hamiltonian is characterized by the intralayer and the interlayer atomic interactions β_i's [Fig. 1(a)], where β_0 represents the nearest-neighbor hopping integral within the same layer; β_1, β_3, and β_4 are between adjacent layers; β_2 and β_5 are associated with the next-nearest layers. β_1 and β_2 are couplings between two vertical sites, and β_3, β_4, and β_5 are nonvertical couplings. The hopping integral values are as follows: $\beta_0 = -3.16$ eV, $\beta_1 = 0.36$ eV, $\beta_2 = -0.01$ eV, $\beta_3 = 0.32$ eV, $\beta_4 = 0.03$ eV, and $\beta_5 = 0.0065$ eV [57].

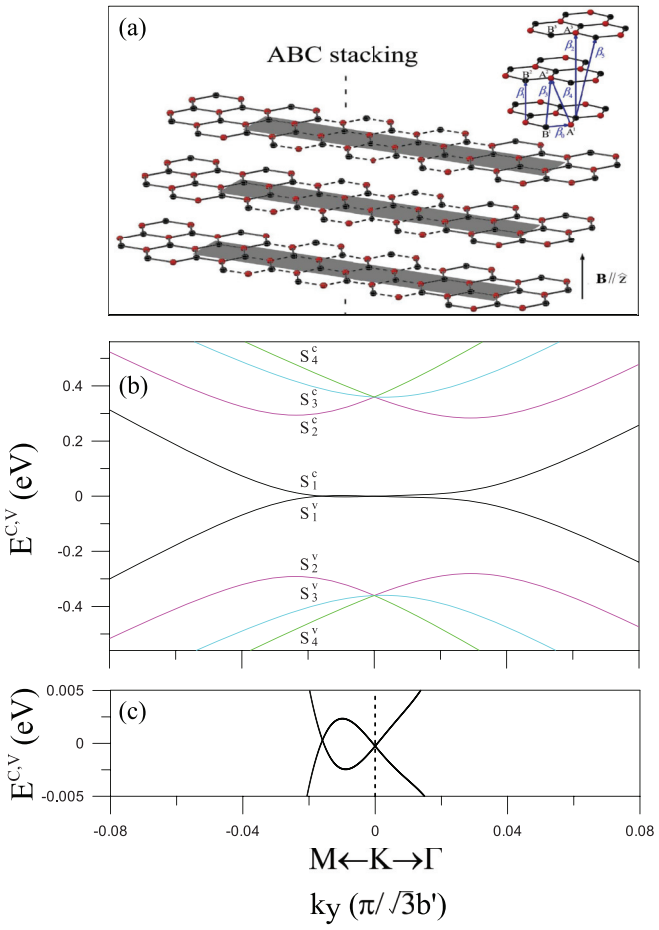

FIG. 1. (Color online) (a) The geometric structure of ABC-stacked graphene under a uniform magnetic field $\mathbf{B} = B_0\hat{z}$, perpendicular to the graphene plane. The interlayer atomic interactions are illustrated in the right panel. At $B_0 = 0$, the low-energy band structure of (b) tetralayer graphene is plotted and (c) shows a zoomed-in view near the Fermi level.

An extra Peierls phase G_R, associated with a uniform perpendicular magnetic field is introduced in the tight-binding functions. Characterized by the vector potential $\mathbf{A}$, G_R takes the form of $(2\pi/\phi_0)\int_{\mathbf{R}}^{\mathbf{r}} \mathbf{A}\cdot d\mathbf{l}$, where $\phi_0(=hc/e)$ is the flux quantum. In the Landau gauge $\mathbf{A} = (0, B_0x, 0)$, the derived period of the Peierls phase along the x axis is $2\phi_0/\phi = 2R_B$. This means that the unit cell is an enlarged rectangle with $4NR_B$ sublattices [the shading of Fig. 1(a)]. The Hamiltonian can be built from the space spanned by the $4NR_B$ tight-binding functions $\{|A^1_{1\mathbf{k}}\rangle, |B^1_{1\mathbf{k}}\rangle, |A^2_{1\mathbf{k}}\rangle, |B^2_{1\mathbf{k}}\rangle \ldots |A^N_{1\mathbf{k}}\rangle, |B^N_{1\mathbf{k}}\rangle \ldots |A^N_{2R_B\mathbf{k}}\rangle, |B^N_{2R_B1\mathbf{k}}\rangle\}$ based on the periodical atoms in the rectangular unit cell, where the superscript and subscript numbers denote the layer and sublattice numbers, respectively, and $\mathbf{k}$ is the wave vector. By detailed calculations, the Hamiltonian matrix elements associated with the hopping integrals $\beta_i's$ are given by

$$\begin{aligned}\langle B^l_{j\mathbf{k}}|H|A^{l'}_{i\mathbf{k}}\rangle &= \beta_0\Sigma\exp\left[i\mathbf{k}\cdot\left(\mathbf{R}_{\mathbf{A}^{l'}_{\mathbf{i}}} - \mathbf{R}_{\mathbf{B}^{l}_{\mathbf{j}}}\right) + \frac{2\pi i}{\Phi_0}\left(G_{R_{B^l_j}} - G_{R_{A^{l'}_i}}\right)\right] \\ &= \beta_0(t_{1,i}\delta_{i,j} + q\delta_{i,j+1})\delta_{l,l'} \quad \text{for} \quad l = 3n-2 \leqslant N, \quad (1)\end{aligned}$$

$$\langle B^l_{j\mathbf{k}}|H|A^{l'}_{i\mathbf{k}}\rangle = \beta_0(t_{3,i}\delta_{i,j-1} + q\delta_{i,j})\delta_{l,l'} \quad \text{for} \quad l = 3n-1 \leqslant N, \quad (2)$$

$$\langle B^l_{j\mathbf{k}}|H|A^{l'}_{i\mathbf{k}}\rangle = \beta_0(t_{2,i}\delta_{i,j} + q\delta_{i,j+1})\delta_{l,l'} \text{ for } l = 3n \leqslant N, \quad (3)$$

$$\langle A^l_{j\mathbf{k}}|H|B^{l'}_{i\mathbf{k}}\rangle = \beta_1\delta_{i,j}\delta_{l,l'-1} \text{ for } l \leqslant N-1, \quad (4)$$

$$\langle B^l_{j\mathbf{k}}|H|A^{l'}_{i\mathbf{k}}\rangle = \beta_2\delta_{i,j}\delta_{l,l'-2} \text{ for } l \leqslant N-2, \quad (5)$$

$$\langle A^l_{j\mathbf{k}}|H|B^{l'}_{i\mathbf{k}}\rangle = \beta_3(t_{2,i}\delta_{i,j} + q\delta_{i,j+1})\delta_{l,l'+1} \quad \text{for} \quad l = 3n-1 \leqslant N, \quad (6)$$

$$\langle A^l_{j\mathbf{k}}|H|B^{l'}_{i\mathbf{k}}\rangle = \beta_3(t_{3,i}\delta_{i,j-1} + q\delta_{i,j})\delta_{l,l'+1} \quad \text{for} \quad l = 3n+1 \leqslant N, \quad (7)$$

$$\langle A^l_{j\mathbf{k}}|H|B^{l'}_{i\mathbf{k}}\rangle = \beta_3(t_{1,i}\delta_{i,j} + q\delta_{i,j+1})\delta_{l,l'+1} \text{ for } l = 3n \leqslant N, \quad (8)$$

$$\langle B^l_{j\mathbf{k}}|H|B^{l'}_{i\mathbf{k}}\rangle = \langle A^{l+2}_{j\mathbf{k}}|H|B^{l'+2}_{i\mathbf{k}}\rangle = \beta_4(t_{1,i}\delta_{i,j} + q\delta_{i,j+1})\delta_{l,l'-1} \quad \text{for} \quad l = 3n-2 \leqslant N, \tag{9}$$

$$\langle A^l_{j\mathbf{k}}|H|A^{l'}_{i\mathbf{k}}\rangle = \langle B^{l+1}_{j\mathbf{k}}|H|B^{l'+1}_{i\mathbf{k}}\rangle = \beta_4(t_{3,i}\delta_{i,j-1} + q\delta_{i,j})\delta_{l,l'-1} \quad \text{for} \quad l = 3n-2 \leqslant N, \tag{10}$$

$$\langle A^l_{j\mathbf{k}}|H|A^{l'}_{i\mathbf{k}}\rangle = \langle B^{l+1}_{j\mathbf{k}}|H|B^{l'+1}_{i\mathbf{k}}\rangle = \beta_4(t_{2,i}\delta_{i,j} + q\delta_{i,j+1})\delta_{l,l'-1} \quad \text{for} \quad l = 3n-1 \leqslant N, \tag{11}$$

$$\langle B^l_{j\mathbf{k}}|H|B^{l'}_{i\mathbf{k}}\rangle = \langle A^{l+2}_{j\mathbf{k}}|H|A^{l'+2}_{i\mathbf{k}}\rangle = \langle A^{l'+1}_{j\mathbf{k}}|H|B^{l+1}_{i\mathbf{k}}\rangle = \beta_5(t_{2,i}\delta_{i,j} + q\delta_{i,j+1})\delta_{l,l'+2} \text{ for } l = 3n \leqslant N, \tag{12}$$

$$\langle A^l_{j\mathbf{k}}|H|A^{l'}_{i\mathbf{k}}\rangle = \langle B^{l+1}_{j\mathbf{k}}|H|B^{l'+1}_{i\mathbf{k}}\rangle = \langle A^{l'+2}_{j\mathbf{k}}|H|B^{l+2}_{i\mathbf{k}}\rangle = \beta_5(t_{1,i}\delta_{i,j} + q\delta_{i,j+1})\delta_{l,l'+2} \text{ for } l = 3n \leqslant N, \tag{13}$$

$$\langle A^l_{j\mathbf{k}}|H|B^{l'}_{i\mathbf{k}}\rangle = \langle B^{l'+2}_{j\mathbf{k}}|H|B^{l+2}_{i\mathbf{k}}\rangle = \langle A^{l'+1}_{j\mathbf{k}}|H|A^{l+1}_{i\mathbf{k}}\rangle = \beta_5(t_{3,i}\delta_{i,j-1} + q\delta_{i,j})\delta_{l,l'-2} \quad \text{for} \quad l = 3n-2 \leqslant N, \tag{14}$$

where n is a positive integer. The four independent phase terms are

$$\begin{aligned} t_{1,i} &= \exp\{i[-(k_x b'/2) - (\sqrt{3}k_y b'/2) + \pi\Phi(i-1+1/6)]\} \\ &\quad + \exp\{i[-(k_x b'/2) + (\sqrt{3}k_y b'/2) \\ &\quad - \pi\Phi(i-1+1/6)]\}, \\ t_{2,i} &= \exp\{i[-(k_x b'/2) - (\sqrt{3}k_y b'/2) + \pi\Phi(i-1+3/6)]\} \\ &\quad + \exp\{i[-(k_x b'/2) + (\sqrt{3}k_y b'/2) \\ &\quad - \pi\Phi(i-1+3/6)]\}, \\ t_{3,i} &= \exp\{i[-(k_x b'/2) - (\sqrt{3}k_y b'/2) + \pi\Phi(i-1+5/6)]\} \\ &\quad + \exp\{i[-(k_x b'/2) + (\sqrt{3}k_y b'/2) \\ &\quad - \pi\Phi(i-1+5/6)]\}, \quad \text{and} \\ q &= \exp\{ik_x b'\}. \end{aligned}$$

In order to enhance the computation efficiency, we choose the bases of $\{|A^1_{1k}\rangle, |B^2_{1k}\rangle, |A^3_{1k}\rangle, |B^1_{1k}\rangle, |A^2_{1k}\rangle, |B^3_{1k}\rangle \ldots |B^1_{2R_Bk}\rangle, |A^2_{2R_Bk}\rangle, |B^3_{2R_B1k}\rangle\}$ to arrange the Hamiltonian as a bandlike symmetric matrix. This allows an efficient numerical solution of the eigenvalues and eigenfunctions, even for a small magnetic field strength and a huge R_B.

In a magnetically enlarged unit cell, the Landau wave function is a linear combination of the products between the subenvelope function and the tight-binding function of each sublattice site, expressed as

$$|\Psi_{\mathbf{k}})\rangle = \sum_{l=1}^{N}\sum_{m=1}^{2R_B} A^l_m|\ A^l_{m\mathbf{k}}\rangle + B^l_m|\ B^l_{m\mathbf{k}}\rangle, \tag{15}$$

where the value of the subenvelope function A^l_m or B^l_m (x-dependent) represents the probability amplitude of the tight-binding function. The LL spectrum is obtained from the diagonalization scheme with a bandlike tight-binding Hamiltonian. The generalized tight-binding model, based on the subenvelope functions of the distinct sublattices, is suitable for studying arbitrarily stacked graphene systems and other layered systems with complicated stacking configurations. This method has been used to define the quantum number of the LLs in monolayer, bilayer, and trilayer graphenes [28,30,31], and is valuable in understanding other physical properties, such as the mechanisms of magneto-optical and Coulomb excitations, etc. [26,33,35,51].

III. RESULTS AND DISCUSSION

A. Zero-field band structure and the quantized Landau levels

The tetralayer ABC-stacked graphene, as a model study, presents a band structure consisting of four pairs of conduction and valence subbands, respectively, labeled $S^{c,v}_1$, $S^{c,v}_2$, $S^{c,v}_3$, and $S^{c,v}_4$, and colored by black, red, blue, and green in Fig. 1(b), respectively. Near $E_F = 0$, the two bands cross in the KM and $K\Gamma$ directions [Fig. 1(c)]; the anisotropic energy dispersion reflects the trigonal warping effect [30]. The states in the vicinity of the weak dispersions are formed predominantly from the atomic orbitals localized on the two outermost layers [19–21]. Away from $E_F = 0$, the conduction (valence) subbands cross near the energy of β_1 ($-\beta_1$). In particular, the subband $S^c_2(S^v_2)$ is mexican-hat shaped and has a local energy minimum (maximum) and maximum (minimum), evaluated respectively, at 0.29 (−0.29) eV and 0.36 (−0.36) eV. The other two pairs, $S^{c,v}_3$ and $S^{c,v}_4$, are monotonic parabolic and linear energy bands. The feature-rich band structure determines the unique field-dependent energy spectra of LLs.

For a tetralayer graphene subjected to $B_0 = 25$ T, the LLs can be divided into four groups, as indicated by black, red, blue and green colors in Fig. 2(a), the division being in accordance with the characteristics of the spatial distribution of the wave function. Moreover, each level is fourfold degenerate for each (k_x, k_y) state. In particular, the extreme values and dispersion relations of the zero-field energy bands are relevant to the onset energies and level spacings for all groups, respectively. The first group starts to form near $E_F = 0$, in the vicinity of which the four LLs are slightly split by the interlayer hoppings, similar to those in trilayer graphene [30], while away from $E_F = 0$ the spacing is apparent and the conduction LL formation is more intensive with increasing energy due to the higher density of states of subband S^c_1. Near β_1, the LLs are densely packed as a consequence of the crossover of the S^c_2, S^c_3, and S^c_4 subbands. The second, third, and forth groups sequentially appear. The spacing for each group also grows in sequence from the lower- to the higher-order groups, corresponding to the energy dispersions of those subbands.

Here, we define the quantum number for each LL based on the Landau wave function, as shown in Fig. 2, where the subenvelope functions of distinct sublatices expressed in Eq. (15) are plotted. The fourfold degenerate Landau wave functions are localized at four different locations in

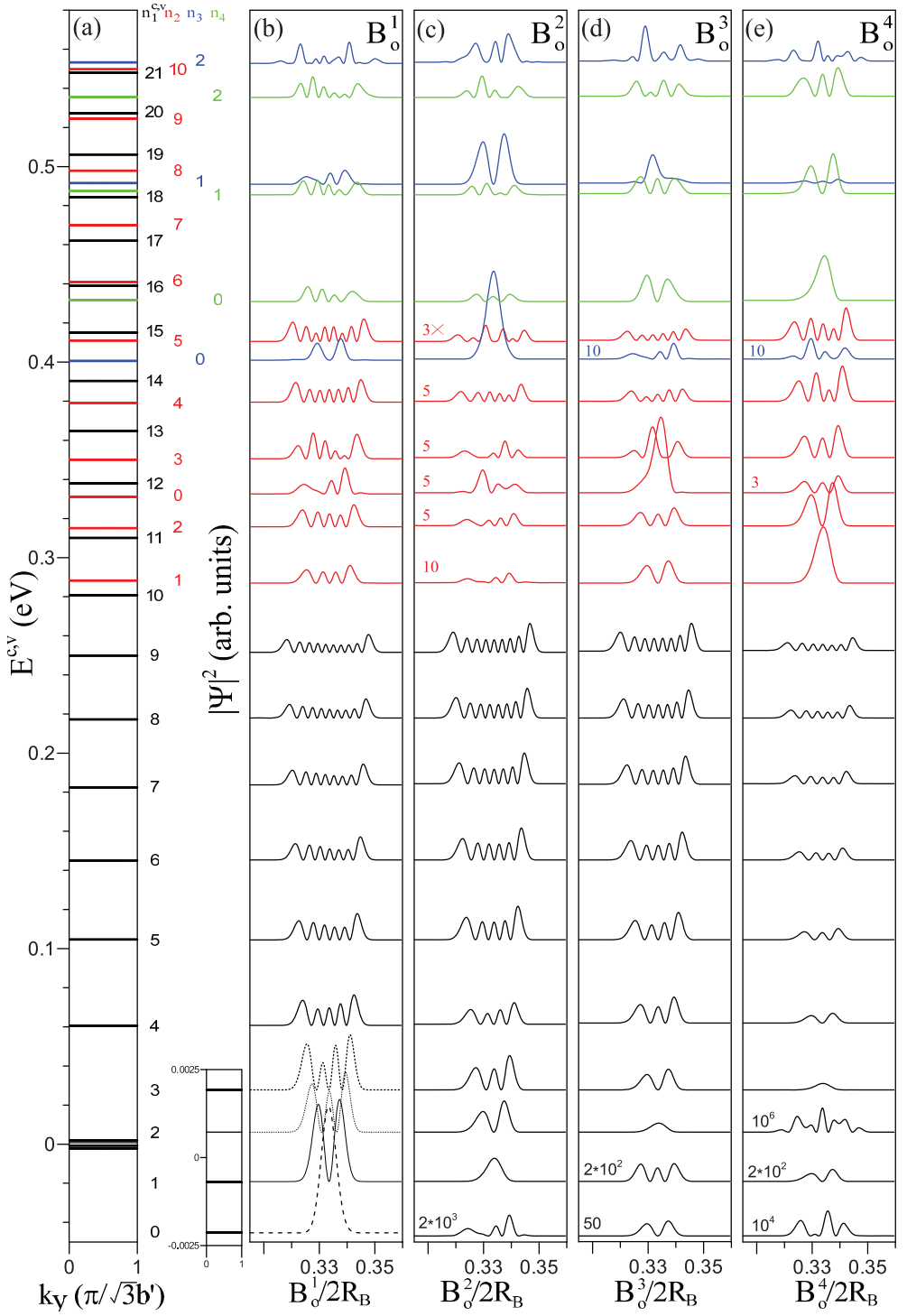

FIG. 2. (Color online) The Landau levels corresponding to (a) tetralayer graphene under $B_0 = 25$ T. For each level, the odd-indexed envelop functions of sublattices B_o^1, B_o^2, B_o^3, and B_o^4 are shown in (b), (c), (d), and (e), respectively.

the enlarged rectangular, i.e., the locations at 1/6, 2/6, 4/6, and 5/6 of the total length of the enlarged cell for the ($k_x = 0, k_y = 0$) state. The wave functions at 1/6 and 4/6 have identical amplitudes, as do those at 2/6 and 5/6. Moreover, the 1/6 localized state has the subenvelope functions A_o^l's ($l = 1,2,3$ and 4 for layer numbers), which are equal to $-B_o^l$'s ($l = 4,3,2$ and 1) of the 2/6 localized state and vice versa. In Figs. 2(b)–2(e), the subenvelop functions of the 2/6 localized state are demonstrated, where only B_o^l is considered, and thus further discussions of only the odd-indexed sublattices are appropriate due to the relationship $B_o^l = -B_e^l$. It is shown that each sublattice component resembles the nth-order Hermite polynomial H_n multiplied by a Gaussian function, a result that is similar to the Landau states in 2D electron gas systems. In principle, the node number n, i.e., the zero points of functions, standing for the spatial symmetry, is used to define the quantum

number of a LL. Be aware of the deformity of the Hermite function, which can be attributed to the complex interlayer atomic interactions.

For the four LLs nearest to $E_F = 0$, the two lower-energy ones of them are occupied valence states, assigned the quantum numbers $n_1^v = 0$ and $n_1^v = 1$, and the other two, belonging to unoccupied conduction states, correspond to $n_1^c = 2$ and 3. As illustrated by the black curves in Fig. 2(b), these numbers are determined by subenvelope function B_o^1 because its weight is evidently stronger than the others. This quantization is responsible for the localized states on the sublattice B^1 of the outer surface. On the contrary, the quantization related to the opposite outmost sites of A^4 is introduced to the other degenerate states. With increasing energy, the higher conduction LL indices increase in order from 4, 5, 6 . . . , with the numbers indicating the zero points of B_o^1. In this same way, the opposite valence LLs are also assigned quantum numbers 4, 5, 6 . . . , with an increase of the number signifying an approach to deep levels.

Instead of a monotonic sequence, an unusual LL sequence accounting for the mexican-hat structure of the S_2^c subband is revealed in the second group. The first conduction LL stems from states being aggregated near the local energy maximum of the S_2^c subband at the K point ($E^c \approx 0.36$ eV). Its quantum number $n_2^c = 0$ is clearly demonstrated by B_o^3, the red curve in Fig. 2(d). The two conduction LLs with $n_2^c = 1$ and 2 are formed between the local minimum and maximum of the S_2^c subband. It is not until the LLs move above $E^c(n_2^c = 0)$ that the quantum numbers grow with the energy due to the monotonically increasing energy dispersions. The valence LLs show a similar sequence. The formation of LLs within this region is dominated by the interplay of the magnetic field strength and the mexican-hat band structure. That is to say, the numbers, energies, and existence of these unusually sequenced LLs strongly depend on B_0. Furthermore, the distorted Landau wave functions for the $n_2^c = 0$ and 3 states mainly result from the intragroup anticrossing of the $n_2^c = 0$ and 3 LLs (illustrated later). Associated with the unique mexican-hat structure, the special spectral patterns also hold for all ABC-stacked graphenes. Unlike the other groups, the conduction and valence quantum numbers of both the third and fourth group LLs are in monotonic sequences, and their onset energies approach the band minimum at the K point. The lowest three conduction LLs of the former, $n_3^c = 0$, 1, and 2, are evident in the B^2 sublattice [blue curves in Fig. 2(c)], as are those of the latter by the B^4 sublattice [green curves in Fig. 2(e)]. The $n_4^c = 2$ LL also shows intergroup anticrossing (between the fourth and the second group) according to the distorted subenvelope functions. Overall, the dominant sublattices are, respectively, B^1, B^3, B^2, and B^4 for the groups changing from the first to the fourth. If there exists a way of identifying the sublattice dominance with respect to each group of LLs, then each sublattice equally dominates in the magnetoelectronic properties. This deduced generalization is applicable to arbitrarily stacked graphenes.

B. Landau-level spectra with respect to different stackings

The unique spectral features for the ABC-stacked configuration is better understood by investigating the dependence of the four grouped LL energies on the magnetic field. As shown by Fig. 3(a), the first group of LLs monotonically depends on B_0, and each moves towards $E_F = 0$ when B_0 approaches zero. In this vicinity, the first four LLs are confined within a small range. The total number and energy distributions of such levels are related to the stacking layers and the interlayer atomic interactions. A more detailed investigation will be made later. On the other hand, in Fig. 3(b), the onset energies of all the other groups correspond to the local extreme values of the subbands S_2^c, S_3^c, and S_4^c at the K point where the subbands cross each other. The mexican-hat dispersion at zero field is evidently reflected in the LL spectrum at lower fields, a complicated pattern showing a nonmonotonic energy dependence on field strength and, therefore, the intragroup LL crossing and anticrossing patterns. The inverted curvature of such a subband structure gives rise to the inverted LL energy dependence. The LLs of the second group at first decrease with the field strength. Upon reaching the minimum of the energy distribution, which is related to the subband minimum, they convert back to the typical behavior regarding B_0. These unusual LLs are reduced by a further increase of field strength. Once the magnetic field is strong enough, i.e., $B_0 > B_c \simeq 15$ T, the first few LLs can accommodate all the electronic states covered by the mexican-hat band structure so that the LLs evolve into an ascending sequence with increasing quantum number. That is to say, the degeneracy of the lowest few levels is comparable to the electronic states enclosed in this region.

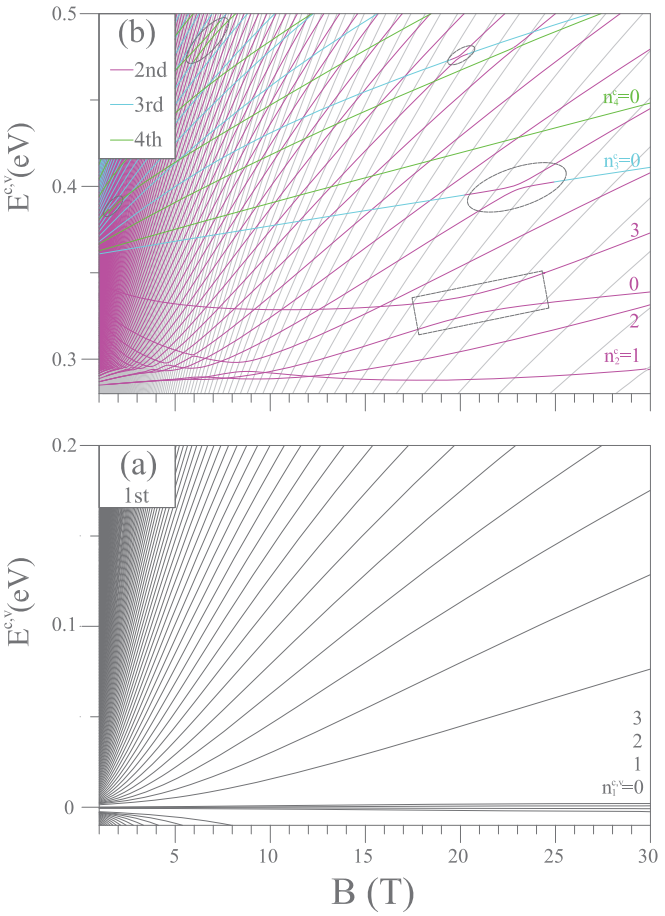

FIG. 3. (Color online) The Landau-level spectrum of ABC-stacked tetralayer graphene.

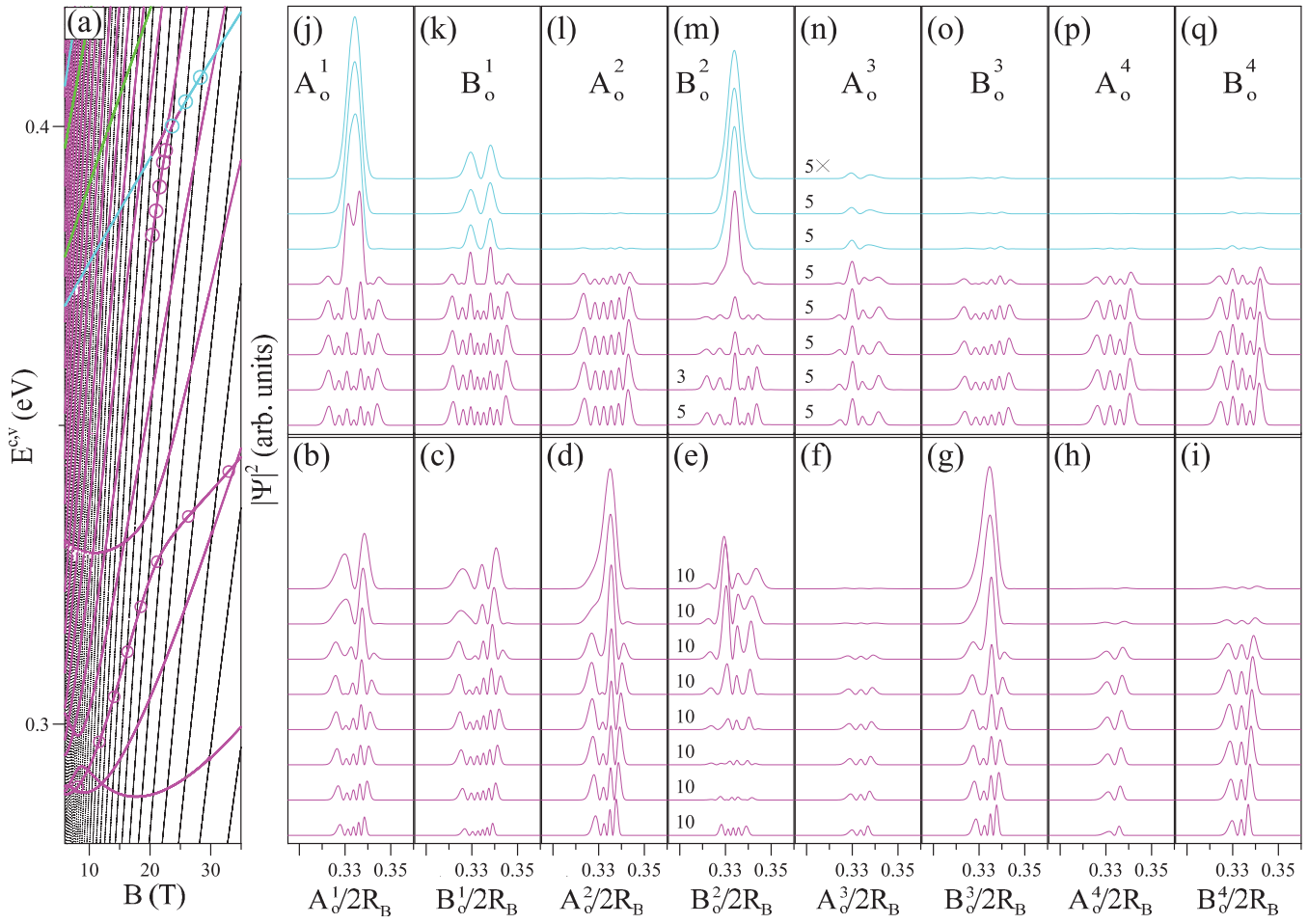

FIG. 4. (Color online) (a) Intragroup and intergroup Landau-level anticrossing patterns. The evolutions of subenvelope functions are demonstrated during the anticrossing processes for (b)–(i) self-group (the second group) and (j)–(q) intergroup (the second and the third groups) Landau levels.

The field-dependent energy spectrum exhibits some special phenomena, including the intragroup and intergroup LL anticrossings. For $B_0 < B_c$, the anticrossing frequently happens for the second group of LLs within 0.29–0.36 eV, for which the levels are in an unusual sequence, e.g., the anticrossing of $n_2^c = 0$ and 3 shown by the dashed rectangle. With increased energy, the anticrossing also occurs between neighboring groups, as in the region of the dashed ellipses. Furthermore, the event can even be triggered between all different groups in a sufficiently strong magnetic field. Through the qualitative perturbation analysis that has been performed on the AB-stacked bulk graphite [56], the Landau states can be correlated to one another by an identifiable pattern of the mode differences between the same sublattice in multiples of 3. The interlayer atomic interaction β_3 between the nonvertical sites in adjacent layers is exclusive to the intergroup anticrossings of the AB-stacked systems. On the other hand, in addition to β_3, there are other interlayer atomic interactions, β_2 and β_5, that are identified to induce both the intragroup and intergroup LL anticrossings in the ABC-stacked graphenes. The energy correction caused by β_2 is its expectation value between the subenvelope functions B^1 and A^3 of the two states possessing the same zero mode. A likewise explanation of the β_3-induced correction is applicable to β_5, which is also responsible for the corrected energy due to the specific relationship between B^1 and B^3; A^1 and A^3.

Some parts of the hybridized Landau states have the same modes, which prevent the mixed LLs crossing each other. The drastic changes of the wave functions during the anticrossing processes between intragroup LLs ($n_2^c = 0$ and 3) and between intergroup LLs ($n_2^c = 5$ and 0) are, respectively, illustrated in Figs. 4(b)–4(i) and 4(j)–4(q). In principle, for Landau states away from the anticrossing regions, the two envelop functions established on the perpendicular projected sublattices in adjacent layers have the same number of the zero points, and the number difference between two sublattices in the same layer is equal to one, except that some of the sublattice amplitudes approach zero for the lowest few LLs of each group. As to the $n_2^c = 3$ wave function at 8 T $< B_0 <$ 14 T [the first four circles in Fig. 4(a)], the well-defined zero points in the lower part of Figs. 4(b)–4(i) are 4, 5, 3, 4, 2, 3, 1, and 2 in the order of $\{A_o^1, B_o^1, A_o^2, B_o^2, A_o^3, B_o^3, A_o^4, B_o^4\}$. However, it starts to mix with the $n_2^c = 0$ Landau wave function as the two LLs, $n_2^c = 0$ and 3, repel each other, and significant hybridization of the two levels is present at the center of the anticrossing region [$\sim$0.29–0.36 eV in Fig. 4(a)], as shown in the middle part of

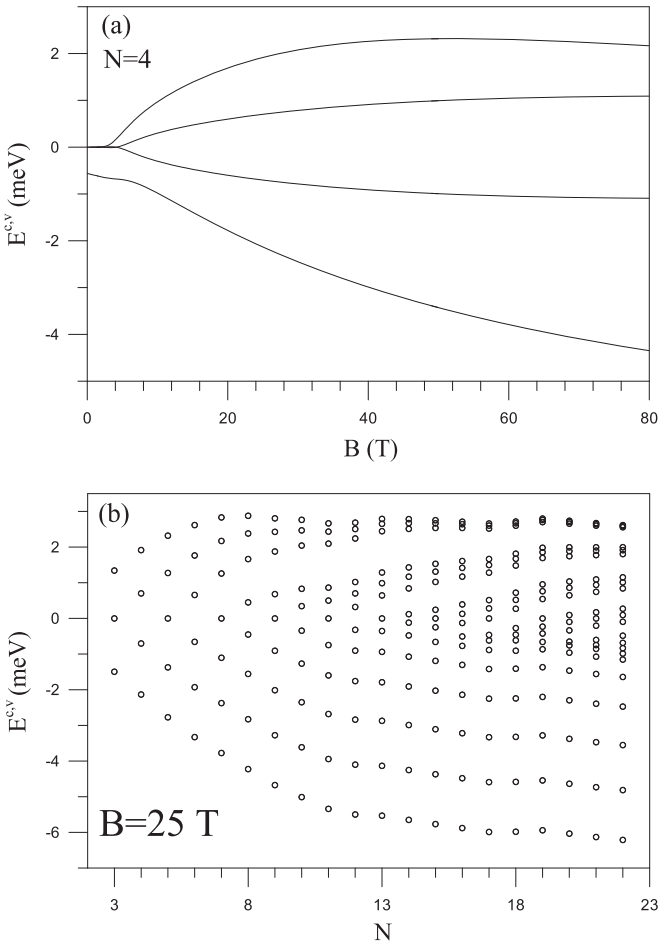

FIG. 5. The field-dependent energies of the four Dirac-point related Landau levels of ABC-stacked tetralayer graphene are shown in (a). In (b), energies are plotted for $B_0 = 25$ T based on their dependence on the number of stacked layers.

Figs. 4(b)–4(i). The amplitudes of the two hybridized states are comparable, while the wave function during the movement away from this region transforms into the characteristics of the $n_2^c = 0$ Landau state. This means that instead of being specific to a certain quantum number, the Landau states in the anticrossing regions are characterized by multi-zero points due to the hybridization of LLs.

Similarly, the interlayer-induced anticrossing between the intergroup LLs, $n_2^c = 5$ and $n_3^c = 0$, also holds, while the coupling modulo is 6 [Figs. 4(j)–4(q)]. Therefore the field-range of anticrossing is of an order smaller than in the above case. By definition of the quantum number for the four grouped LLs, the two correlated Landau states are deduced to satisfy the following conditions: $n_1^c - n_2^c = \pm 3n$, $n_1^c - n_3^c = \pm(3n-2)$, $n_1^c - n_4^c = \pm 3n$, $n_2^c - n_3^c = \pm(3n-1)$, $n_2^c - n_4^c = \pm(3n-1)$, and $n_3^c - n_4^c = \pm(3n-1)$. The multimode Landau wave function implies that a substitution of a single-mode wave function in the Hamiltonian fails to exactly solve the eigenenergy and to realize the stacked graphene systems.

Another important feature of the tetralayer graphene is its four LLs near $E_F = 0$. A zoomed-in view on the region of the interest is shown in Fig. 5(a). Within a very narrow energy range, $-4 \sim 2$ meV, the degeneracy of LLs is weakly lifted by interlayer atomic interactions, and the B_0-dependent energies of the splitting LLs are dominated by the specific interaction β_4. When B_0 approaches zero, the four levels are directly mapped to the four separate Dirac points in terms of their energies [Fig. 1(c)]—the energies that are relevant to the stacking configurations. Moreover, the generalization of the Dirac-point related LLs is extended to the N-layer ABC-stacked graphenes. It is shown that in Fig. 5(b), there exist N fourfold degenerate LLs, with their energies insensitive to B_0 and limited within a very narrow region near $E_F = 0$. The energy width is evaluated to be $\sim$10 meV for $N \gtrapprox 10$. The above discussed characteristics of the LL spectrum are also formed in systems with different stacking sequences, e.g., in AA- and AB- stacked graphenes; however, the energy distributions of these $4N$ LLs and the groups that they could be classified into strongly depend on stacking configurations.

A further exploration on the cases of distinct graphene layers is worthwhile in order to comprehend the LL anticrossings and the unusually sequenced LLs. For an N-layer ABC-stacked graphene, there are $N-1$ pairs of conduction and valence subbands intersecting near the energies $\pm\beta_1$ [17]. The dispersion and number of the mexican-hat energy subbands determine the unique LL patterns. There is only one such group of LLs in the trilayer graphene [Fig. 6(a)], and the group number becomes two for both the pentalayer and hexalayer graphenes [Figs. 6(b) and 6(c)]. However, the trilayer graphene exhibits a relatively narrow inverted region of LLs, which means that the states enclosed in the mexican-hat band structure are relatively small, as is the estimated critical magnetic field B_c. It can be deduced that with an increased number of layers, more groups demonstrate the intragroup LL anticrossing and own stronger B_c's; the anticrossing regions are also enlarged. The derived rules are that the number of groups is, respectively, $(N-1)/2$ and $(N-2)/2$ for odd and even N's. The aforementioned results apparently reveal the feature-rich spectrum for more stacking layers.

The stacking symmetry plays an important role in the LL spectrum features of multilayer graphenes, such as the sublattice dominance in Landau states, the field-dependent energies and the inter- and intragroup LL anticrossings. For an AA-stacked tetralayer graphene, the LLs are divided into four groups, with group possessing a monolayer-like spectrum, as shown in Fig. 7. The LL distributions of the four groups are related to the four Dirac cones that are primarily separated by interlayer atomic interaction α_1 (the case without the field seen in Ref. [13]). The LL distribution regarding the same group is almost symmetric about the zero-mode Dirac-point related LL, which is almost constant as a function of field strength, and each level moves towards the Dirac point when the magnetic field approaches zero. The quantum numbers of LLs can be classified by sublattice A or B in any layer, since the four layers are equivalent and each reflects the same relationship between the two subenvelope functions described for a monolayer graphene. Meanwhile, each Landau state can be characterized by a harmonic function with a single mode, since there is no coupling among LLs resulting from interlayer atomic interactions. This demonstrates that neither the inter- nor the intragroup LL anticrossings can occur regardless of the circumstances in terms of energies and field strengths.

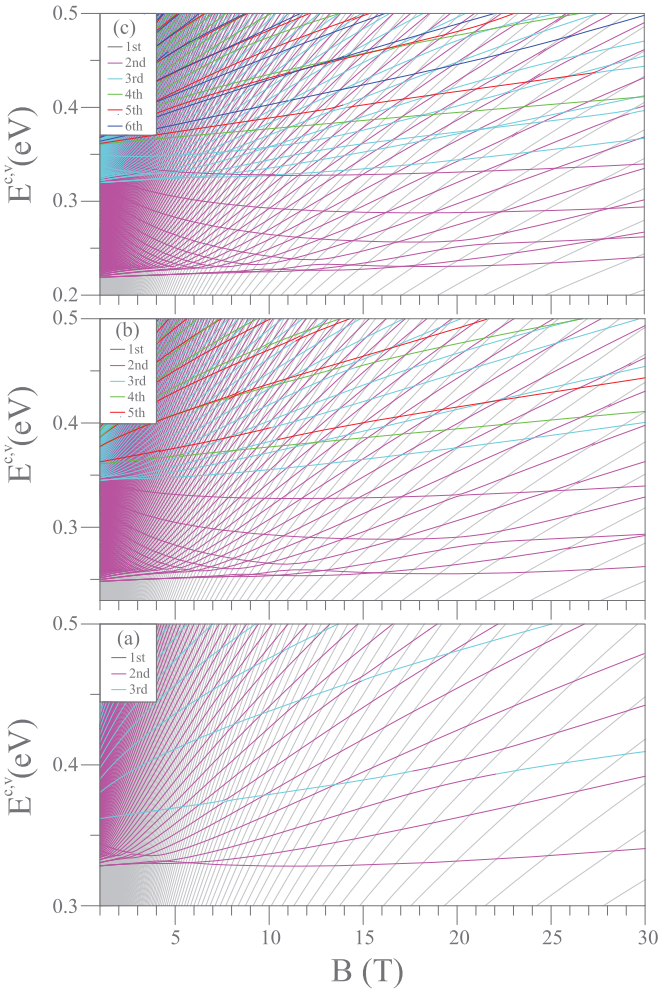

FIG. 6. (Color online) The Landau-level spectra of ABC-stacked (a) trilayer, (b) pentalayer, and (c) hexalayer graphenes.

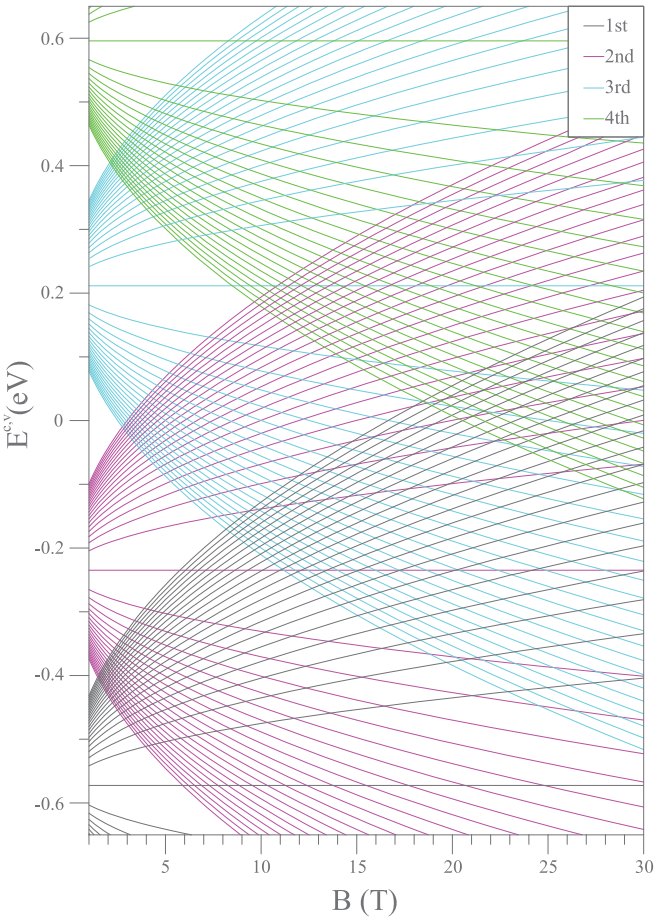

FIG. 7. (Color online) The Landau-level spectrum of AA-stacked tetralayer graphene.

The four groups of LLs exhibited in AB-stacked graphenes are rather more distinct than those formed in AA- and ABC-stacked graphenes, as shown in Fig. 8. The dominant subenvelop functions in the first to fourth group determine the quantum numbers and, respectively, correspond to sublattices $A^2(B^3)$, $B^1(A^4)$, $A^1(B^4)$, and $B^2(A^3)$. However, similar to the AA- and ABC-stacked configurations, there are four fourfold degenerate LLs with their energies insensitive to the magnetic field. They are located in the vicinity of $E_F = 0$, and categorized as the first and the second groups assigned the quantum numbers $n_1^v = 0$, $n_1^v = 1$, $n_2^c = 0$, and $n_2^c = 1$. The intergroup LL anticrossing occurs around two neighboring groups, i.e., one case is between the first and the second groups, and another case between the second and the third groups, as seen in the regions marked by the ellipses. Two levels based on the rules $n_1^c - n_2^c = \pm 3$ and $n_2^c - n_3^c = \pm 4$, respectively, are introduced in the former and the latter cases. It is the neighboring interlayer atomic interaction γ_3 that leads to the couplings for these LLs [29]. However, unlike the situation in the ABC-stacked graphenes, the anticrossing between LLs rarely occurs between intergroups.

A generalization of magnetoelectronic properties is valuable for understanding other physical properties, such as the mechanisms of magneto-optical excitations. Previous works investigated the feature-rich magneto-absorption spectra of AA- and AB-stacked graphenes [26,35]. The intragroup LL transitions satisfy the particular selection rule $\Delta = \pm 1$ (the same as that of monolayer graphene), whereas the rules for intergroup transitions depend on the configuration. The intergroup transitions are forbidden due to the derived zero electric dipole moments in the AA-stacked system. Also, for AB-stacked graphenes with an odd layer, the excitations from the quantized LLs of the linear bands to those of the parabolic bands are forbidden. On the other hand, the strong effects of the anticrossing LLs on the absorption spectra are quite different from those of the well-behaved LLs [51]. The hybridization of the LLs induces new optical selection rules of modulo 3 in addition to the $\Delta = \pm 1$ well applied to transitions between the well-defined LLs. Especially mandated is a need to focus on the intra-second group transitions under magnetic fields weaker than the critical strength, where the frequently appearing anticrossings lead to a considerable amount of peaks with intensities associated with the LL hybridization. Further and thorough investigations of the optical response of ABC-stacked graphenes is worthwhile.

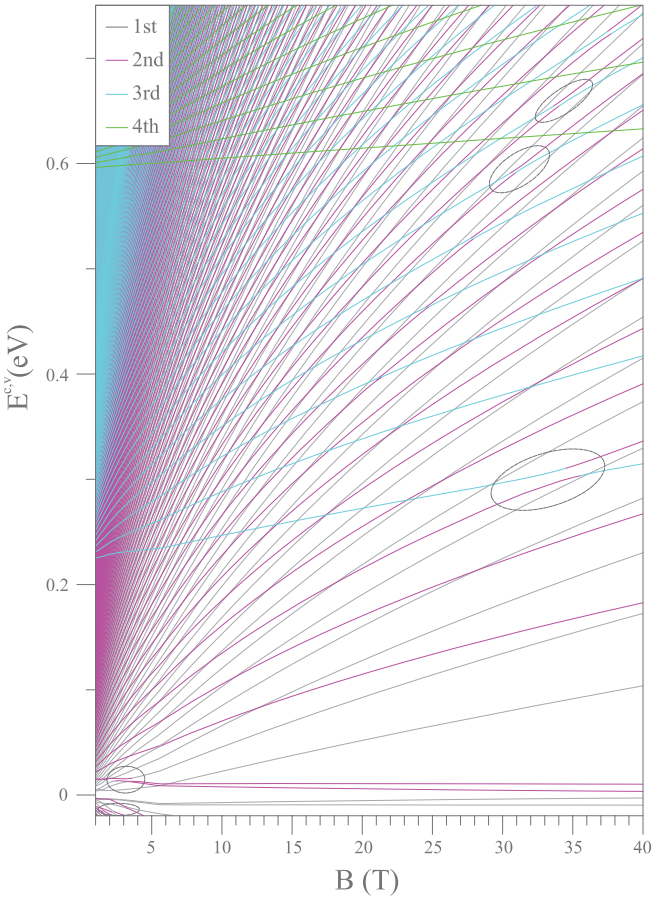

FIG. 8. (Color online) The Landau-level spectrum of AB-stacked tetralayer graphene.

IV. CONCLUSION

The generalized tight-binding model is developed to elucidate the magnetoelectronic properties of multilayer graphenes. Particularly depending on the layer number and stacking configuration, the feature-rich characteristics include the sublattice dominance, the field-dependent energies and inter- and intragroup anticrossings. For an N-layer graphene, the LLs are clearly classified into N groups, of which each onset energy and the field-dependent LL energies are relevant to the zero-field band structure; the relationship between the subenvelop functions of the $2\times N$ sublattices is specific for the associated stacking configuration. The spatial distributions of the subenvelope functions are critical in describing the electronic properties, some of which, such as the quantum numbers and group classifications, can be determined by the numbers of the zero points and the dominant sublattices. This method provides an approach to describing other stacking graphene systems.

For ABC-stacked graphenes, an increased versatility of magnetoelectronic properties is observed for a higher number of layers, and the classification of groups is straightforward. There is a total number of $4N$ LLs with a narrow energy width ($\sim$10 meV) near $E_F = 0$ that reflect the Dirac points. They all belong to the first group, with one half being completely filled and the other half empty. In other stacking configurations, such field-insensitive LLs are also observed, while their classification and energy distributions are different. In AA-stacked graphenes, for example such LLs corresponds to the zero-mode levels of distinct groups, with LL energies largely separated by the interlayer atomic interaction α_1. Although these LLs are also confined nearly $E_F = 0$, they belong to the first few groups in AB-stacked graphenes.

The phenomenon of inter- and intragroup LL anticrossings, detailing the electronic properties, is strikingly pronounced in ABC-stacked graphenes. The former appears frequently between neighboring groups, and even between remote ones under a sufficiently strong field. The signature of the latter results from the densely inverted LLs in the spectrum, which is attributed to the higher number of mexican-hat energy subbands in the zero-field case. However, the groups of the unusually sequenced LLs and the intragroup anticrossings start to disappear at a critical field strength B_C, with B_C being higher if the number of layers is higher. On the contrary, AB-stacked multilayer graphenes occasionally show anticrossings only between neighboring groups, and AA-stacked graphenes present no anticrossings from either the same or different groups. In addition to the nonvertical hopping integral between two adjacent layers, two hopping integrals from next-neighboring layers also combine the LLs in the 3 modulo for ABC-stacked graphenes. This is attributed to the specific relationship between the subenvelope functions and the interlayer atomic interactions. Furthermore, this hybridization of the LLs is expected to enrich the physical properties, such as the magneto-optical properties and the quantum Hall effects in the multilayer graphenes.

ACKNOWLEDGMENTS

This work was supported in part by the Ministry of Science and Technology of Taiwan, the Republic of China, under Grants No. NSC 102-2112-M-006-007-MY3 and No. NSC 102-2112-M-165-001-MY3.

[1] K. S. Novoselov, A. K. Geim, S. V. Morozov, D. Jiang, Y. Zhang, S. V. Dubonos, I. V. Grigorieva, and A. A. Firsov, Science **306**, 666 (2004).

[2] K. S. Novoselov, D. Jiang, F. Schedin, T. J. Booth, V. V. Khotkevich, S. V. Morozov, and A. K. Geim, Proc. Natl. Acad. Sci. USA **102**, 10451 (2005).

[3] J. K. Lee, S. C. Lee, J. P. Ahn, S. C. Kim, J. I. B. Wilson, and P. John, J. Chem. Phys. **129**, 234709 (2008).

[4] A. C. Ferrari, J. C. Meyer, V. Scardaci, C. Casiraghi, M. Lazzeri, F. Mauri, S. Piscanec, D. Jiang, K. S. Novoselov, S. Roth, and A. K. Geim, Phys. Rev. Lett. **97**, 187401 (2006).

[5] A. Reina, X. Jia, J. Ho, D. Nezich, H. Son, V. Bulovic, M. S. Dresselhaus, and J. Kong, Nano Lett. **9**, 30 (2009).

[6] L. Liu, H. Zhou, R. Cheng, W. J. Yu, Y. Liu, Y. Chen, J. Shaw, X. Zhong, Y. Huang, and X. Duan, ACS Nano. **6**, 8241 (2012).

[7] C. H. Lui, Z. Li, Z. Chen, P. V. Klimov, L. E. Brus, and T. F. Heinz, Nano Lett. **11**, 164 (2011).

[8] S. Hattendorf, A. Georgi, M. Liebmann, and M. Morgenstern, Surf. Sci. **610**, 53 (2013).

[9] L. G. Cancadoa, K. Takaia, T. Enokia, M. Endob, Y. A. Kimb, H. Mizusakib, N. L. Spezialic, A. Jorioc, and M. A. Pimenta, Carbon **46**, 272 (2008).

[10] A. J. Cooper, N. R. Wilson, I. A. Kinloch, and R. A. W. Dryfe, Carbon **66**, 340 (2014).

[11] W. Norimatsu and M. Kusunoki, Phys. Rev. B **81**, 161410 (2010).

[12] A. Gruneis, C. Attaccalite, L. Wirtz, H. Shiozawa, R. Saito, T. Pichler, and A. Rubio, Phys. Rev. B **83**, 165429 (2011).

[13] C. W. Chiu, S. C. Chen, Y. C. Huang, F. L. Shyu, and M. F. Lin, Appl. Phys. Lett. **103**, 041907 (2013).

[14] A. Grüneis, C. Attaccalite, L. Wirtz, H. Shiozawa, R. Saito, T. Pichler, and A. Rubio, Phys. Rev. B **78**, 205425 (2008).

[15] E. McCann and M. Koshino, Rep. Prog. Phys. **76**, 056503 (2013).

[16] C. L. Lu, C. P. Chang, Y. C. Huang, J. M. Lu, C. C. Hwang, and M. F. Lin, J. Phys.: Condens. Matter **18**, 5849 (2006).

[17] R. Xiao, F. Tasnádi, K. Koepernik, J. W. F. Venderbos, M. Richter, and M. Taut, Phys. Rev. B **84**, 165404 (2011).

[18] K. F. Mak, J. Shan, and T. F. Heinz, Phys. Rev. Lett **104**, 176404 (2010).

[19] F. Guinea, A. H. CastroNeto, and N. M. R. Peres, Phys. Rev. B **73**, 245426 (2006).

[20] N. B. Kopnin, T. T. Heikkila, and G. E. Volovik, Phys. Rev. B **83**, 220503 (2011).

[21] H. Wang, J.-H. Gao, and F.-C. Zhang, Phys. Rev. B **87**, 155116 (2013).

[22] A. H. Castro Neto, F. Guinea, N. M. R. Peres, K. S. Novoselov, and A. K. Geim, Rev. Mod. Phys. **81**, 109 (2009).

[23] T. Ohta, A. Bostwick, J. L. McChesney, T. Seyller, K. Horn, and E. Rotenberg, Phys. Rev. Lett **98**, 206802 (2007).

[24] E. Moreau, S. Godey, X. Wallart, I. Razado-Colambo, J. Avila, M.-C. Asensio, and D. Vignaud, Phys. Rev. B **88**, 075406 (2013).

[25] C. Coletti, S. Forti, A. Principi, K. V. Emtsev, A. A. Zakharov, K. M. Daniels, B. K. Daas, M. V. S. Chandrashekhar, T. Ouisse, D. Chaussende, A. H. MacDonald, M. Polini, and U. Starke, Phys. Rev. B **88**, 155439 (2013).

[26] Y. H. Ho, J. Y. Wu, R. B. Chen, Y. H. Chiu, and M. F. Lin, Appl. Phys. Lett. **97**, 101905 (2010).

[27] E. McCann and V. I. Fal'ko, Phys. Rev. Lett. **96**, 086805 (2006).

[28] Y. H. Lai, J. H. Ho, C. P. Chang, and M. F. Lin, Phys. Rev. B **77**, 085426 (2008).

[29] M. Koshino and E. McCann, Phys. Rev. B **83**, 165443 (2011).

[30] C. H. Ho, Y. H. Ho, Y. H. Chiu, Y. N. Chen, and M. F. Lin, Ann. Phys. **326**, 721 (2011).

[31] C. P. Chang, C. L. Lu, F. L. Shyu, R. B. Chen, Y. K. Fang, and M. F. Lin, Carbon **42**, 2975 (2004).

[32] S. H. R. Sena, J. M. Pereira, Jr, F. M. Peeters, and G. A. Farias, Phys. Rev. B **84**, 205448 (2011).

[33] J. Y. Wu, S. C. Chen, O. Roslyak, G. Gumbs, and M. F. Lin, ACS Nano **5**, 1026 (2011).

[34] Y. E. Lozovik and A. A. Sokolik, Nano Res. Lett. **7**, 134 (2012).

[35] Y. H. Ho, Y. H. Chiu, D. H. Lin, C. P. Chang, and M. F. Lin, ACS NANO. **4**, 1465 (2010).

[36] H. J. van Elferen, A. Veligura, N. Tombros, E. V. Kurganova, B. J. vanWees, J. C. Maan, and U. Zeitler, Phys. Rev. B **88**, 121302 (2013).

[37] K. S. Novoselov, A. K. Geim, S. V. Morozov, D. Jiang, M. I. Katsnelson, I. V. Grigorieva, S. V. Dubonos, and A. A. Firsov, Nature (London) **438**, 197 (2005).

[38] Y. B. Zhang, Y. W. Tan, H. L. Stormer, and P. Kim, Nature (London) **438**, 201 (2005).

[39] K. S. Novoselov, E. McCann, S. V. Morozov, V. I. Fal'ko, M. I. Katsnelson, U. Zeitler, D. Jiang, F. Schedin, and A. K. Geim, Nat. Phys. **2**, 177 (2006).

[40] T. Taychatanapat, K. Watanabe, T. Taniguchi, and P. Jarillo-Herrero, Nat. Phys. **7**, 621 (2011).

[41] L. Zhang, Y. Zhang, J. Camacho, M. Khodas, and I. Zaliznyak, Nat. Phys. **7**, 953 (2011).

[42] C. L. Lu, C. P. Chang, Y. C. Huang, R. B. Chen, and M. L. Lin, Phys. Rev. B **73**, 144427 (2006).

[43] O. Taisuke, B. Aaron, and S. Thomas, Science **313**, 951 (2006).

[44] J. B. Oostinga, H. B. Heersche, X. Liu, A. F. Morpurgo, and L. M. K, Nat. Mater. **7**, 151 (2008).

[45] Y. Zhang, T. T. Tang, C. Girit, Z. Hao, M. C. Martin, A. Zettl, M. F. Crommie, Y. R. Shen, and F. Wang, Nature (London) **459**, 820 (2009).

[46] E. V. Castro, K. S. Novoselov, S. V. Morozov, N. M. R. Peres, J. M. B. dosSantos, J. Nilsson, F. Guinea, A. K. Geim, and A. H. Castro Neto, Phys. Rev. Lett. **99**, 216802 (2007).

[47] C. L. Lu, C. P. Chang, Y. C. Huang, J. H. Ho, C. C. Hwang, and M. F. Lin, J. Phys. Soc. Jpn. **76**, 024701 (2007).

[48] M. F. Craciun, S. Russo, M. Yamamoto, J. B. Oostinga, A. F. Morpurgo, and S. Tarucha, Nat. Nanotechnol. **4**, 383 (2009).

[49] M. Yankowitz, F. Wang, C. N. Lau, and B. J. Le Roy,Phys. Rev. B **87**, 165102 (2013).

[50] M. Kindermann and E. J. Mele, Phys. Rev. B **84**, 161406 (2011).

[51] Y.-H. Ho, S.-J. Tsai, M.-F. Lin, and W.-P. Su, Phys. Rev. B **87**, 075417 (2013).

[52] T. Morimoto and M. Koshino, Phys. Rev. B **87**, 085424 (2013).

[53] M. Serbyn and D. A. Abanin, Phys. Rev. B **87**, 115422 (2013).

[54] E. A. Henriksen, D. Nandi, and J. P. Eisenstein, Phys. Rev. X **2**, 011004 (2012).

[55] Y. Lee, J. Velasco, D. Tran, F. Zhang, W. Bao, L. Jing, K. Myhro, D. Smirnov, and C. N. Lau, Nano Lett. **13**, 1627 (2013).

[56] M. Inoue, J. Phys. Soc. Jpn. **17**, 808 (1962).

[57] J.-C. Charlier, J.-P. Michenaud, and Ph. Lambin, Phys. Rev. B **46**, 4540 (1992).